PHOTONICS Research

Dead-zone-free atomic magnetometer based on hybrid Poincaré beams

Ke Tian, Weifeng Ding, and Zhaoying Wang*

Zhejiang Province Key Laboratory of Quantum Technology and Device, School of Physics, Zhejiang University, Hangzhou 310027, China
**Corresponding author: zhaoyingwang@zju.edu.cn*

Received 18 January 2024; revised 2 March 2024; accepted 4 March 2024; posted 4 March 2024 (Doc. ID 519409); published 1 May 2024

In this paper, we present the experiment and the theory scheme of light-atom interaction in atomic magnetometers by using a hybrid Poincaré beam (HPB) to solve an annoying problem, named "dead zone." This kind of magnetometer can be sensitive to arbitrary directions of external magnetic fields. The HPB has a complex polarization distribution, consisting of a vector radially polarized beam and a scalar circularly polarized beam in our experiment. These two kinds of beams have different directions of dead zones of external magnetic fields; thereby, the atomic magnetometer with an HPB can avoid the non-signal area when the direction of the external magnetic field is in the plane perpendicular to the light polarization plane. Furthermore, the optical magnetic resonance (OMR) signal using an HPB still has no dead zones even when the direction of the external magnetic field is in the plane parallel to the polarization plane in our scheme. Our work has the potential to simplify and optimize dead-zone-free atomic magnetometers. © 2024 Chinese Laser Press

https://doi.org/10.1364/PRJ.519409

1. INTRODUCTION

Optically pumped magnetometers (OPMs) have sensitivity up to sub-femto-tesla by measuring the Zeeman splitting caused by the external static magnetic fields and even can be comparable with superconducting quantum interference devices (SQUIDs) [1]. With the developments in sensitivity [2–5] and stability [6,7], OPMs have been widely used in fundamental physics [8,9], biomagnetism [10,11], geomagnetism [12], and magnetic fields measurement in space [13], like detecting dark matters [14].

"Dead zone" is an inherent flaw of optically pumped magnetometers, shown as the vanished sensitivity in certain directions of the external magnetic fields [15]. These annoying dead zones can be effectively solved by adding the signals of two beams with different linear polarization directions [16], combining unpolarized light and spatially varying microwave fields based on the symmetry of atomic transition hyperfine structure [17], utilizing both resonance signals at the Larmor frequency and its second harmonics [18], adjusting the direction of the linear polarization to be perpendicular to the external magnetic field in Bell-Bloom magnetometers [19], synchronously maintaining the linear polarization and the RF field to be perpendicular to the external magnetic field in RF magnetometers [20], using a Herriott cavity [21], and modulating the ellipticity of the light polarization [22,23]. Most of the above solutions are based on modulating the types or the directions of the polarization of the light beam, which arouses interest in whether dead-zone-free measurement can be achieved by using a single hybrid Poincaré beam (HPB) as a pump-probe beam without any modulations.

The HPB is one vector polarized beam (VPB) with a complex polarization structure in the transverse direction on a hybrid-order Poincaré sphere [24,25]. The hybrid-order Poincaré sphere can describe an arbitrary polarization of beam with a vortex phase, except the North Pole [26,27]. The interaction of the vector polarization beams and atoms is an emerging area of research [28–30] since the VPBs provide the additional degrees of manipulation freedom of the beam and the atomic media [31]. The interactions can be used in the measurement of the strength [32,33] and the direction [34,35] of the magnetic fields. Furthermore, the interaction can be applied in mapping the polarization distribution [36], extraction of the spatial optical information [37], and optical tweezers [38,39].

Recently, radially or azimuthally polarized beams, as two types of the VPBs, have been introduced in the magnetic measurement in magnetometers by our group [40]. Radially or azimuthally polarized beams have diverse directions of the magnetic fields in the dead zones compared with linearly or circularly polarized beams. On the condition of this kind of beams, some unusual features appear but dead zones still exist, which means more complex VPBs in dead-zone-free measurement are promising.

In this paper, we extend our previous work based on radially or azimuthally polarized beams and demonstrate a single-beam magnetometer scheme with an HPB in varying directions of the external magnetic fields. First, several optical magnetic

resonance (OMR) signals based on HPBs with different polarization distributions in varying external magnetic fields perpendicular to the polarization plane are demonstrated experimentally, which explores that sensitivity in arbitrary directions of external magnetic fields is possible. We also derive the analytical expressions to describe the results, and the experimental results fit well with the theoretical results. The OMR signals under the situation in which external magnetic fields are parallel to the polarization plane of light are also detected to prove that the all-space dead-zone-free measurement can be achieved. We think our work brings the vector polarized beams into dead-zone-free measurement and has the potential to simplify and optimize all-direction atomic magnetometers.

2. THEORETICAL MODEL

The polarization of HPBs is described by extending the Jones vectors and the Poincaré sphere to hybrid order orbital angular momentum versions [26,27]. We use a fundamental-mode Gaussian beam and a Laguerre-Gaussian beam as the two eigenstates of HPBs, and the Jones vector can be written as [24]

$$E_{\mathrm{HPB}} = [-i\sin\gamma - \sin(2\psi-\gamma)]\mathrm{LG}_{0,0}(\hat{e}_x + i\hat{e}_y) + [\cos\gamma - i\cos(2\psi-\gamma)]\mathrm{LG}_{0,2}(\hat{e}_x - i\hat{e}_y), \quad (1)$$

where $\mathrm{LG}_{0,l}$ means the lth-order Laguerre-Gaussian function. γ and ψ are two tunable parameters. Based on this, two new parameters need to be defined to characterize the proportions of 0th-order Laguerre-Gaussian beams (0-LGB) and 2nd-order Laguerre-Gaussian beams (2-LGB):

$$N = -i\sin\gamma - \sin(2\psi-\gamma), \qquad S = \cos\gamma - i\cos(2\psi-\gamma). \quad (2)$$

To combine this expression with the polarization distributions on the hybrid Poincaré sphere, we define

$$\theta = 2\arctan\left(\frac{|S|}{|N|}\right), \qquad \Phi = \arg[S] - \arg[N]. \quad (3)$$

Here, θ and Φ correspond to the coordinate on the hybrid Poincaré sphere, as shown in Fig. 1. Also, Fig. 1 shows the polarization distributions of HPBs at different positions of the hybrid Poincaré sphere, $(\theta,\Phi) = (0°,0°), (64°,0°), (90°,0°), (102°,0°), (110°,0°)$, and $(180°,0°)$ in order A to F, and A', C', and F' are the phase profiles of A, C, and F, respectively. When $\theta = 0°$, the beam shows a scalar circularly polarized beam type, as shown in Fig. 1 panel A. When $\theta = 90°$, it means that the proportions of the 0-LGB and the 2-LGB are the same, as shown in Fig. 1 panel C; the beam has equal components of the center left-handed circular polarization and the outer ring right-handed circular polarization, which presents a vector radially polarized distribution. By controlling the value of γ and ψ, the beams with arbitrary polarization distributions on the hybrid Poincaré sphere can be prepared.

As known, elliptically polarized beams are the combinations of linearly polarized beams and circularly polarized beams. Linearly polarized beams and circularly polarized beams are special cases in which the polarization ellipticity is equal to 0 and 1, respectively. We define a similar equivalent ellipticity R_{cy} in HPBs to describe the proportions of the radially polarized beam component (Fig. 1 panel C) and the circularly polarized beam component (Fig. 1 panel A). When the equivalent ellipticity changes from 0 to 1, the beam changes from a vector radially polarized beam to a scalar circularly polarized beam. Based on Eqs. (1) and (2), considering the relationship between the polarization and the proportion of the 0- or 2-LGB, the equivalent ellipticity can be expressed as

$$R_{\mathrm{cy}} = 1 - \frac{\mathrm{Min}[|N|^2,|S|^2]}{\mathrm{Max}[|N|^2,|S|^2]}. \quad (4)$$

Here, $\mathrm{Min}[|N|^2,|S|^2]$ and $\mathrm{Max}[|N|^2,|S|^2]$ represent the minimum and maximum values between $|N|^2$ and $|S|^2$, respectively.

Then, we deeply consider how the beams with such polarization distributions interact with atoms. In a thermatomic ensemble of limited size, the polarization of the beams acting on

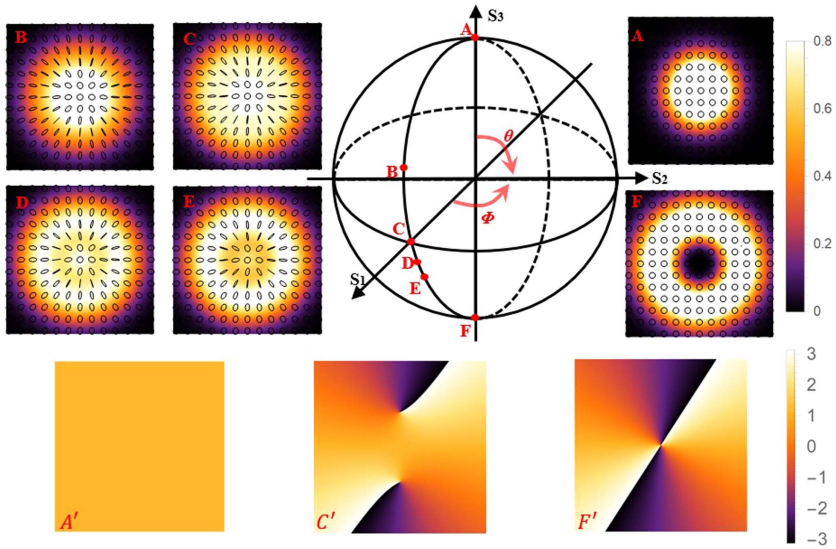

Fig. 1. The hybrid Poincaré sphere and the polarization distributions. A–F: (0°, 0°), (64°, 0°), (90°, 0°), (102°, 0°), (110°, 0°), and (180°, 0°) in order. A', C', and F' are the phase profiles of A, C, and F, respectively.

the atoms is the result of all polarization synthesis. To describe the problem more clearly, we define the beam propagation axis as the Z-axis and the polarization plane as the X-Y plane. First, we take the situation that the direction of the external magnetic field is in the plane perpendicular to the polarization plane as an example. In our previous work, for a vector radially or azimuthally polarized beam, the normalized amplitude of the OMR absorption signal has a magnetic angular dependence, which is written as $h_{cy}(\varphi) = \frac{1}{4}(3\cos^2\varphi - 1)^2$ [40]; here, φ means the angle between the beam propagation axis (Z-axis) and the direction of the external magnetic fields (in the X-Z plane). That work also shows that radially or azimuthally polarized beams have the same direction as the dead zone, which means the change of the angle Φ in the Poincaré sphere does not affect the direction of the dead zone. So only the change of the angle θ in the Poincaré sphere is considered in our following discussion. For circularly polarized beams, the normalized amplitude of the absorption signal with the magnetic angular dependence can be written as $h_{ci}(\varphi) = \cos^2\varphi$ [40]. Now, for the HPBs the normalized amplitude with the magnetic angular dependence can be given as

$$h_{HPB}(\varphi) = (1 - R_{cy}) \cdot h_{cy}(\varphi) + R_{cy} \cdot h_{ci}(\varphi). \quad (5)$$

The angle between the beam propagation axis and the direction of the external magnetic field in the dead zone is named a magic angle. The magic angle of circularly polarized beams is 90°, while that of vector radially polarized beams is $\arccos(\sqrt{1/3}) \approx 54.7°$ (and 125.3°). To focus on these two specific directions, $h_{HPB}(90°)$ and $h_{HPB}(54.7°)$ are discussed to show the variation of the signal strength with the beam polarization.

As shown in Fig. 2, when $R_{cy} = 1$, which means a magnetometer with circularly polarized pumped beam, the dipole moment of the atomic ensemble at 90° loses its effect, and the atoms cannot be optically polarized; then the signal of OMR $h_{HPB}(90°)$ is zero. But at 54.7° the atoms can be optically polarized, and $h_{HPB}(54.7°)$ is nonzero. Further, when $R_{cy} = 0$, which means a magnetometer with radially polarized pumped beam, the atomic quadrupole moment at 54.7° loses its effect, and then $h_{HPB}(54.7°)$ is zero, but $h_{HPB}(90°)$ is nonzero. If $R_{cy} \neq 0$ and 1, $h_{HPB}(54.7°)$ and $h_{HPB}(90°)$ are both nonzero because the HPB has the proportions of the radially polarized beam component and the circularly polarized beam component, which have different magic angles. With the increase of the equivalent ellipticity, the amplitude at 90° decreases while the amplitude at 54.7° increases all the time. Even more, if $R_{cy} = 3/7$, the amplitude of two angles can attain the same value of 0.14. In a word, the magnetometer with HPB has no dead zone since the dipole moment and quadrupole moment can compensate each other in some special directions of the magnetic field.

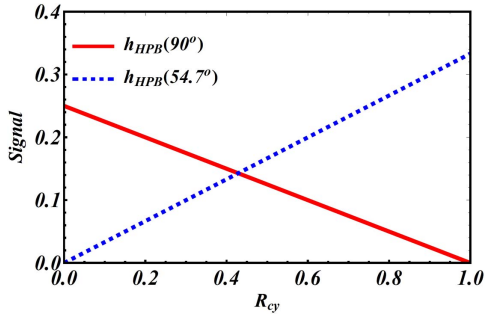

Fig. 2. The normalized absorption signal amplitude at 90° and 54.7° as a function of the equivalent ellipticity.

3. EXPERIMENTAL SETUP

Our experimental setup is shown in Fig. 3, which is the single-beam magnetometer with an RF field. The laser beam is generated by a tunable single-mode diode laser (Toptica's DL pro), whose wavelength is tuned near the 780.2 nm D2 line of ^{87}Rb ($5^2S_{1/2}$, $F = 2 \rightarrow 5^2P_{3/2}$, $F' = 1$). At first, a half-wave plate (HWP1) and a polarization beam splitter (PBS1) are used to adjust the intensity of the pump-probe beam. Then, the beam passes a half-wave plate (HWP2) and a quarter-wave plate (QWP1) and can be converted to any polarization on the hybrid Poincaré sphere. The angles between the optical axis of the HWP2 and QWP1 and the horizontal direction are γ and ψ, respectively, which have been mentioned in Eq. (1). Next, the beam is sent into the Sagnac interferometer, which is made up of a PBS (PBS2), a spatial light modulator (SLM), and a mirror (M). Figure 3(b) shows the phase diagram loading by the SLM. Finally, the beam passes a quarter-wave plate (QWP2), whose optical axis is 45° from the horizontal direction. Hereto, HPBs with different polarization distributions, as Fig. 1 shows, are generated. To block stray light and sieve the HPB with a ideal polarization, we set an aperture (A) to limit the diameter of the spot. The intensity of the beam is about 35 μW. At last, the HPB passing through the Rb atom cell is detected by a photodiode (PD).

The Rb cell, which is paraffin coated with 5 cm in length and 3.5 cm in diameter, is put in a four-layer μ-metal magnetic shield to avoid the influence of the environmental magnetic fields. The experiment is performed at room temperature (about 20°C). A solenoid coil inside the shield produces a uniform magnetic field along the beam propagation direction (Z-axis). Three pairs of Helmholtz coils are used to generate a 5000 nT stable magnetic field in any direction, and a 35 kHz RF field perpendicular to the external magnetic field is also prepared.

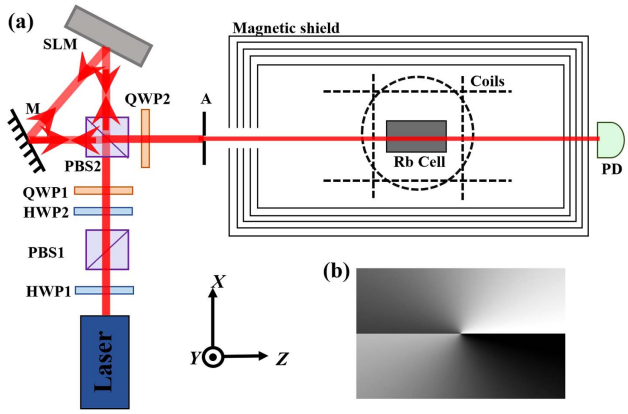

Fig. 3. (a) Schematic of the experimental setup. (b) The phase diagram loading by SLM. HWP: half-wave plate; PBS: polarization beam splitter; QWP: quarter-wave plate; M: mirror; A: aperture; SLM: spatial light modulator; PD: photodiode.

4. RESULTS AND DISCUSSION

We define the amplitude of the OMR signal as the value of the peak depth of the absorption line of the transmitted beams. Next, we will mainly explore the change of the OMR signal amplitude in the HPB systems as a function of the varying angle φ of the external magnetic fields in the *X-Z* plane.

In Figs. 4(a) and 4(b), the OMR signal amplitude as a function of the angle φ of five kinds of beams has been explored theoretically and experimentally, respectively. The theoretical result in Fig. 4(a) is calculated based on Eq. (5) with different θ. The direction of θ determines the value of R_{cy}, which means different proportions of the radially polarized beam component and the circularly polarized beam component. When $R_{cy} \neq 0$ ($\theta \neq 90°$) and $R_{cy} \neq 1$ ($\theta \neq 0°, 180°$), the HPBs can achieve dead-zone-free measurement. The five beams have different polarization distributions as θ equals 0°, 64°, 90°, 102°, and 110°. For comparison, all the results have been normalized. The inset pictures represent the proportion of the intensity distribution of the 0-LGB, the 2-LGB, and the whole beam in order. The intensity distributions and the line shapes of the results of the theoretical model and the experiment match well, except that the beam spot is not a perfectly circular pattern in the experiment.

In Fig. 4, the line shape with $\theta = 0°$ is the same as the scalar circularly polarized beam type [23,40]. The line shape with $\theta = 90°$ is the same as the vector radially polarized beam type [40]. For other values of θ, they mean the varying polarization distributions consist of different proportions of the vector radial and the scalar circular polarization, corresponding to different line shapes, and the line shapes show sensitivity in arbitrary directions of the external magnetic fields. In the case of θ equal to 110°, the amplitude of the OMR signal can always keep the value larger than 0.1, which means an apparent dead-zone-free measurement.

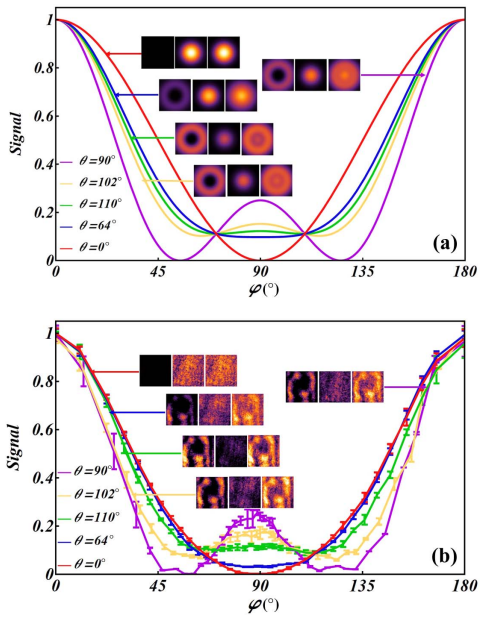

Fig. 4. The amplitude of the OMR signal as a function of the angle between the beam propagation axis and the direction of the external magnetic fields in the *X-Z* plane. The inset pictures represent the proportion of the intensity distribution of the 0-LGB, the 2-LGB, and the whole beam in order. (a) Theoretical results. (b) Experimental results.

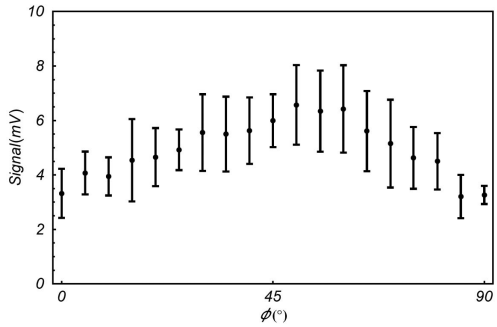

Fig. 5. Amplitude of the OMR signal as a function of the angle ϕ between the beam propagation axis and the direction of the external magnetic fields in the *X-Y* plane.

Finally, we chose the polarization distribution of θ equal to 110° on the hybrid Poincaré sphere as an example to explore the results when the directions of the external magnetic fields are in other planes, for example in the *X-Y* plane.

As Fig. 1 shows, the polarization distributions for B-E positions are radially rotational symmetry, which means the amplitudes of the OMR signals in the planes perpendicular to the *X-Y* plane have the same shape. So, we focus on the OMR signal when the external magnetic fields are in the *X-Y* plane. From Fig. 5, there are always non-zero signals at about 3–6 mV in the *X-Y* plane when the direction of the magnetic field changes from the *X*-axis to the *Y*-axis. That is, our system can achieve dead-zone-free measurement in all directions of the external magnetic fields. It should be mentioned that because the direction of the external magnetic field is not exactly in the *X-Y* plane and the polarization distribution is not entirely ideal, the signal amplitude in Fig. 5 varies in a small range, but theoretically, it should remain constant for different directions of the magnetic field.

Here, we should mention that in the case of the elliptically polarized light, it can be regarded as a combination of linearly and circularly polarized light. When the angle between the beam propagation axis and the direction of the external magnetic fields is in the *X-Z* plane and the *Y-Z* plane, the change rule of the amplitude of the OMR signal is similar to that in the case of HPBs. However, in the *X-Y* plane, the amplitude of the OMR signal equals 0 when $\phi = 54.7°$ because the elliptically polarized light has no symmetrical polarization distribution in the *X-Y* plane as HPBs.

5. CONCLUSION

In this paper, we build a single-beam magnetometer scheme using different kinds of HPBs. The OMR signals based on HPBs with different polarization distributions in varying directions of the external magnetic fields perpendicular to the polarization plane are studied, which can present sensitivity in arbitrary directions of the external magnetic fields. We derived the analytical expressions for these signals, and the experimental results fit well with the theoretical ones. As the equivalent ellipticity changes from 1 to 0, the line shape of

the results changes from the shape of the circularly polarized beam type to the shape of the vortex radially polarized beam type. We also give an example of the result in the *X*-*Y* plane, and there are always non-zero signals in the *X*-*Y* plane when the direction of the magnetic field changes from the *X*-axis to the *Y*-axis, while the atomic magnetometer using elliptically polarized light still shows dead zones. All the results show that such HPBs can achieve dead-zone-free measurement by controlling polarization distributions. In this paper, we bring a new approach to combine the results of two kinds of polarized beams. As the generation methods of vortex beams have been simplified, our system has the potential to simplify and optimize all-direction magnetic measurement atomic magnetometers. It has potential application in biomagnetism and geomagnetism as it is miniaturized and portable.

Funding. National Natural Science Foundation of China (12274366).

Disclosures. The authors declare that there are no conflicts of interest related to this article.

Data Availability. Data underlying the results presented in this paper are not publicly available at this time but may be obtained from the authors upon reasonable request.

REFERENCES

1. D. Budker and M. Romalis, "Optical magnetometry," Nat. Phys. **3**, 227–234 (2007).
2. R. Li, C. Perrella, and A. Luiten, "Repumping atomic media for an enhanced sensitivity atomic magnetometer," Opt. Express **30**, 31752–31765 (2022).
3. C. Troullinou, R. Jimenez-Martinez, J. Kong, *et al.*, "Squeezed-light enhancement and backaction evasion in a high sensitivity optically pumped magnetometer," Phys. Rev. Lett. **127**, 193601 (2021).
4. H. Yao, B. Maddox, and F. Renzoni, "High-sensitivity operation of an unshielded single cell radio-frequency atomic magnetometer," Opt. Express **30**, 42015–42025 (2022).
5. M. Jiang, Y. Qin, X. Wang, *et al.*, "Floquet spin amplification," Phys. Rev. Lett. **128**, 233201 (2022).
6. N. Wilson, P. Light, A. Luiten, *et al.*, "Ultrastable optical magnetometry," Phys. Rev. Appl. **11**, 044034 (2019).
7. X. Zhang, J. Hu, and N. Zhao, "Stable atomic magnetometer in parity-time symmetry broken phase," Phys. Rev. Lett. **130**, 023201 (2023).
8. H. Stækind, K. Jensen, J. H. Müller, *et al.*, "Nonlocal temporal interferometry for highly resilient free-space quantum communication," Phys. Rev. X **13**, 021036 (2023).
9. M. S. Safronova, D. Budker, D. DeMille, *et al.*, "Search for new physics with atoms and molecules," Rev. Mod. Phys. **90**, 025008 (2018).
10. Y. J. Kim, I. Savukov, and S. Newman, "Magnetocardiography with a 16-channel fiber-coupled single-cell Rb optically pumped magnetometer," Appl. Phys. Lett. **114**, 143702 (2019).
11. M. J. Brookes, J. Leggett, M. Rea, *et al.*, "Magnetoencephalography with optically pumped magnetometers (OPM-MEG): the next generation of functional neuroimaging," Trends Neurosci. **45**, 621–634 (2022).
12. F. Pedreros Bustos, D. Bonaccini Calia, D. Budker, *et al.*, "Remote sensing of geomagnetic fields and atomic collisions in the mesosphere," Nat. Commun. **9**, 3981 (2018).
13. M. H. Acuña, "Space-based magnetometers," Rev. Sci. Instrum. **73**, 3717–3736 (2002).
14. S. Afach, B. C. Buchler, D. Budker, *et al.*, "Search for topological defect dark matter with a global network of optical magnetometers," Nat. Phys. **17**, 1396–1401 (2021).
15. A. L. Bloom, "Principles of operation of the rubidium vapor magnetometer," Appl. Opt. **1**, 61–68 (1962).
16. B. Chéron, H. Gilles, J. Hamel, *et al.*, "Improvement of the spatial amplitude isotropy of a ^{4}He magnetometer using a modulated pumping beam," J. Phys. III **7**, 1735–1740 (1997).
17. E. B. Aleksandrov, A. K. Vershovskiĭ, and A. S. Pazgalev, "Magnetometer based on a pair of symmetric transitions in the ^{87}Rb hyperfine structure," Tech. Phys. **51**, 919–923 (2006).
18. G. Bevilacqua and E. Breschi, "Magneto-optic spectroscopy with linearly polarized modulated light: theory and experiment," Phys. Rev. A **89**, 062507 (2014).
19. T. Wu, X. Peng, Z. Lin, *et al.*, "A dead-zone free ^{4}He atomic magnetometer with intensity-modulated linearly polarized light and a liquid crystal polarization rotator," Rev. Sci. Instrum. **86**, 103105 (2015).
20. H. Wang, T. Wu, W. Xiao, *et al.*, "Dual-mode dead-zone-free double-resonance alignment-based magnetometer," Phys. Rev. Appl. **15**, 024033 (2021).
21. Q. Q. Yu, S. Q. Liu, C. Q. Yuan, *et al.*, "Light-shift-free and dead-zone-free atomic-orientation-based scalar magnetometry using a single amplitude-modulated beam," Phys. Rev. Appl. **18**, 014015 (2022).
22. A. Ben-Kish and M. V. Romalis, "Dead-zone-free atomic magnetometry with simultaneous excitation of orientation and alignment resonances," Phys. Rev. Lett. **105**, 193601 (2010).
23. H. Wang, T. Wu, H. Wang, *et al.*, "Magneto-optical spectroscopy with arbitrarily polarized intensity-modulated light in ^{4}He atoms," Phys. Rev. A **101**, 063408 (2020).
24. X. Ling, X. Yi, Z. Dai, *et al.*, "Characterization and manipulation of full Poincaré beams on the hybrid Poincaré sphere," J. Opt. Soc. Am. B **33**, 2172–2176 (2016).
25. Z. Liu, Y. Liu, Y. Ke, *et al.*, "Generation of arbitrary vector vortex beams on hybrid-order Poincaré sphere," Photonics Res. **5**, 15–21 (2017).
26. S. Fu, Y. Zhai, T. Wang, *et al.*, "Tailoring arbitrary hybrid Poincaré beams through a single hologram," Appl. Phys. Lett. **111**, 211101 (2017).
27. X. Yi, Y. Liu, X. Ling, *et al.*, "Hybrid-order Poincaré sphere," Phys. Rev. A **91**, 023801 (2015).
28. C. Rosales-Guzmán, B. Ndagano, and A. Forbes, "A review of complex vector light fields and their applications," J. Opt. **20**, 123001 (2018).
29. Y. Shen, X. Wang, Z. Xie, *et al.*, "Optical vortices 30 years on: OAM manipulation from topological charge to multiple singularities," Light Sci. Appl. **8**, 90 (2019).
30. J. Wang, F. Castellucci, and S. Franke-Arnold, "Vectorial light–matter interaction: exploring spatially structured complex light fields," AVS Quantum Sci. **2**, 031702 (2020).
31. L. Stern, A. Szapiro, E. Talker, *et al.*, "Controlling the interactions of space-variant polarization beams with rubidium vapor using external magnetic fields," Opt. Express **24**, 4834–4841 (2016).
32. S. Qiu, J. Wang, F. Castellucci, *et al.*, "Visualization of magnetic fields with cylindrical vector beams in a warm atomic vapor," Photonics Res. **9**, 2325–2331 (2021).
33. S. Shi, D.-S. Ding, Z.-Y. Zhou, *et al.*, "Magnetic-field-induced rotation of light with orbital angular momentum," Appl. Phys. Lett. **106**, 261110 (2015).
34. Y. Sun and Z. Wang, "Optically polarized selective transmission of a fractional vector vortex beam by the polarized atoms with external magnetic fields," Opt. Express **31**, 15409–15422 (2023).
35. F. Castellucci, T. W. Clark, A. Selyem, *et al.*, "Atomic compass: detecting 3D magnetic field alignment with vector vortex light," Phys. Rev. Lett. **127**, 233202 (2021).
36. J. Wang, Y. Chen, X. Yang, *et al.*, "Optically polarized selection in atomic vapor and its application in mapping the polarization distribution," J. Phys. Commun. **4**, 015019 (2020).
37. J. Wang, X. Yang, Y. Li, *et al.*, "Optically spatial information selection with hybridly polarized beam in atomic vapor," Photonics Res. **6**, 451–456 (2018).
38. L. Zhu, Y. Tai, H. Li, *et al.*, "Multidimensional optical tweezers synthetized by rigid-body emulated structured light," Photonics Res. **11**, 1524–1534 (2023).
39. L. Zhu, M. Tang, H. Li, *et al.*, "Optical vortex lattice: an exploitation of orbital angular momentum," Nanophotonics **10**, 2487–2496 (2021).
40. Y. Ren and Z. Wang, "Opto-magnetic resonance single-beam magnetometer driven by vector polarized light," Opt. Express **31**, 5113–5121 (2023).